The Effects of Dissolved Hydrogen on the Mechanical Properties and Fracture Behavior of SE508 Nitinol Wire For Biomedical Components

A Senior Project

presented to

the Faculty of the Materials Engineering Department

California Polytechnic State University, San Luis Obispo

In Partial Fulfillment

of the Requirements for the Degree

Bachelor of Science

by

Kathryn Meany, Ryan Thompson

June 2023

Acknowledgments

Our team would like to thank the Materials Engineering Department for providing us with the equipment used in the research. We would like to thank our sponsor company, Resonetics Corporations, and our technical contacts Evan Borgeson and Chris Fahey for their expertise in nitinol and processing. In addition, we thank our Senior Project Advisor, Professor Blair London for guiding us through the project.

Abstract

Superelastic nitinol is competitive in the medical device industry due to its unique properties. Typical processing methods, such as electropolishing and etching, can introduce hydrogen into nitinol's microstructure, which is known to affect its tensile properties. Due to the lack of information about hydrogen content in processed nitinol, an experiment was designed to find a relationship between hydrogen content and SE508 nitinol wire's tensile strength, permanent set, ductility, and mode-of-failure of the fracture surface. Using a 50% sulfuric acid to mimic industry practices, five wire samples were exposed to the acid solution at seven different time intervals (ranging from 0 to 60 minutes) with additional groups of three samples at 24 hours and four days. Segments from two samples at each time interval were evaluated for hydrogen content, which revealed a consistent increase in hydrogen with time in the etchant. Each sample was tensile tested at a rate of 5 mm/min. The data showed little change in tensile strength and permanent set due to hydrogen, keeping at a consistent permanent set of around 0.20% and ultimate tensile strength of around 1080MPa. Ductility by measuring maximum elongation did not show a clear negative trend due to hydrogen under 150 wt.ppm. The fracture surfaces were imaged under the SEM, where a mixed mode of failure was characterized above 140 wt.ppm hydrogen. Adding between 0 and 150 wt.ppm hydrogen did not have major effects on the tensile properties of superelastic nitinol but had a noticeable impact on the fracture morphology at high concentrations.

Key Words

Nitinol, superelastic, medical devices, stents, hydrogen content, embrittlement, tensile testing, permanent set, ultimate tensile strength, scanning electron microscopy, local plastic deformation, microvoid coalescence.

Table of Contents

List of Figures

List of Tables

Notation

A_f = austenite finish temperature
A_s = austenite start temperature
M_f = martensite finish temperature
M_s = martensite start temperature
wt.ppm = parts per million by weight
at. %= atomic percent

Introduction

i. History

Nitinol (name derived from Nickel Titanium Naval Ordnance Laboratory) was first developed by William Buehler of the U.S. Naval Ordnance Lab in 1959. Originally, nitinol was promising for its impact resistance and ductility. Nitinol's heat dependence was not documented until 1961, when it was accidentally shown to have temperature-dependent shape-memory after Dr. David Muzzey held his pipe lighter up to the deformed nitinol wire and it miraculously deformed back to its original shape. Dr. Frederick Wang joined Buehler's lab and characterized the mechanism behind nitinol's shape-memory, which would form the fundamentals of nitinol for future research and applications [1].

ii. Composition

Nitinol is an alloy that is, typically, equimolar amounts of nickel and titanium. The alloy has found several applications in medical devices (stenting, guidewires, etc.), where changes in the composition and heat treatments can either make nitinol exhibit shape-memory effects dependent on temperature or superelastic effects that exhibit a change of structure based on an applied load. The exact composition for medical devices, according to ASTM F2063-18, is shown in Table 1 [2]. Many of the elements, excluding nickel and titanium, are considered impurities and affect the shape-memory properties of nitinol heavily [3,4]. Although altering the temperature of M_s is important for developing shape-memory or superelastic nitinol, changing the ratio between nickel and titanium is the preferred method. This way, the alloy can be finely tuned to achieve the desired properties. Notably, oxygen and carbide contaminations produce TiC and $Ti_4Ni_2O_x$, which lead to crack initiation [5].

Table I: Chemical Composition Requirements of Nitinol according to ASTM F2063-18. Any element with *maximum* is impurities from the ore and processing [2]

Element	% (mass/mass)
Nickel	54.5 - 57.0
Carbon, maximum	0.040
Cobalt, maximum	0.050
Copper, maximum	0.010
Chromium, maximum	0.010
Hydrogen, maximum	0.005
Iron, maximum	0.050
Niobium, maximum	0.025
Nitrogen, maximum	0.005
Oxygen, maximum	0.040
Titanium	*Balance*

iii. Crystal Structure

Austenitic nitinol has a structure similar to body-centered cubic (BCC). It is the primary crystal structure above and M_s due to its stability at higher temperatures. Once the nitinol is cooled below M_s, austenite becomes unstable and tends to form a lower-entropy crystal structure. Often, this structure is monoclinic martensite, which has a tetragonal-like crystal structure. This differs from austenite in that there is a 96.8^o slant in the crystal structure. The crystal structure can be observed in **Figure 1** [6]. Note that one side is shorter than the other, resulting in a slanted structure. The transformation occurs using self-accommodating twinning of the lattice structure to produce the martensitic phase, which appears as needle-like crystals. There are no atomic bonds that are broken during the phase transformation, which means the process is reversible [6].

Using the reversible phase-change, important values such as A_s, A_f, M_f, and M_s can be found in ASTM F2004-17. Using differential scanning calorimetry (DSC) shown in **Figure 2**, heating the nitinol from -120^{o}C to 30^{o}C results in a change in heat flow, which correlates to a phase change. The phase changes from martensite to austenite. The A_s and A_f can be found on the graph. A similar peak appears when cooling the alloy back down to low temperatures, which results in a change from austenite to martensite. Like A_s and A_f, M_s, and M_f can be found on the graph in **Figure 2** [7].

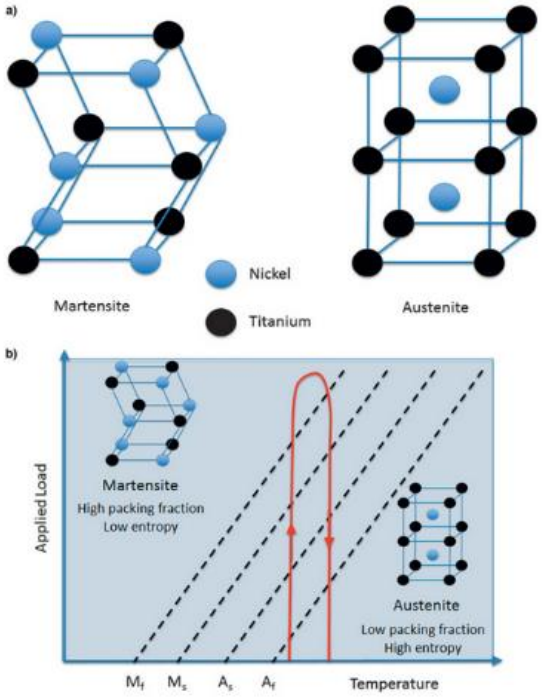

Figure 1: (a) Nitinol crystalline structure in phases Martensite and Austenite and (b) the relationship between austenite and martensite when increasing either load or temperature.

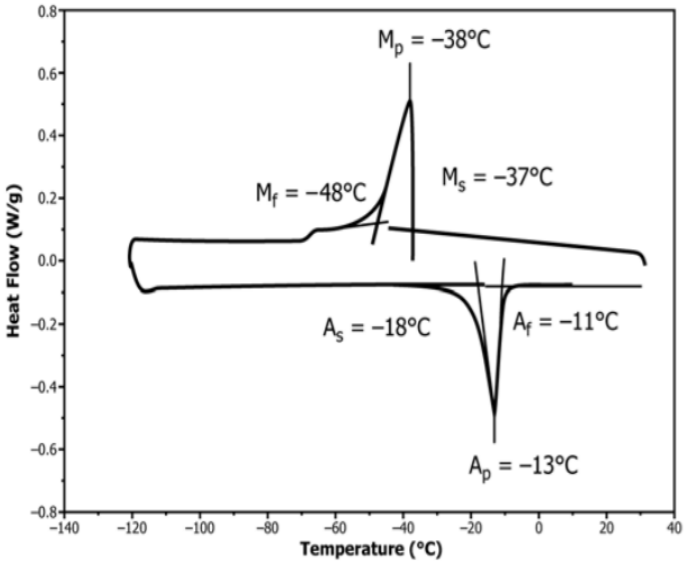

Figure 2: DSC graph of shape-memory nitinol. Because austenitic nitinol has high entropy, it is more stable at higher temperatures. Changing the nickel content can increase the A_f to above room temperature to become superelastic [8,9].

iv. Microstructure

Typically, the composition of nitinol alloys is between 45 at.% and 55 at.% Ni, which lends itself to having a majority NiTi solid solution. Unless the alloy is exactly equi-atomic, precipitates form, shown in the phase diagram in Figure 3. Shape-memory alloys and superelastic alloys can precipitate Ti_2Ni, $TiNi_3$, and Ti_4Ni_3 precipitates, which increase the room-temperature hardness and affect the A_f and M_s [9]. During annealing, the presence of precipitates decreases as the annealing temperature increases [10].

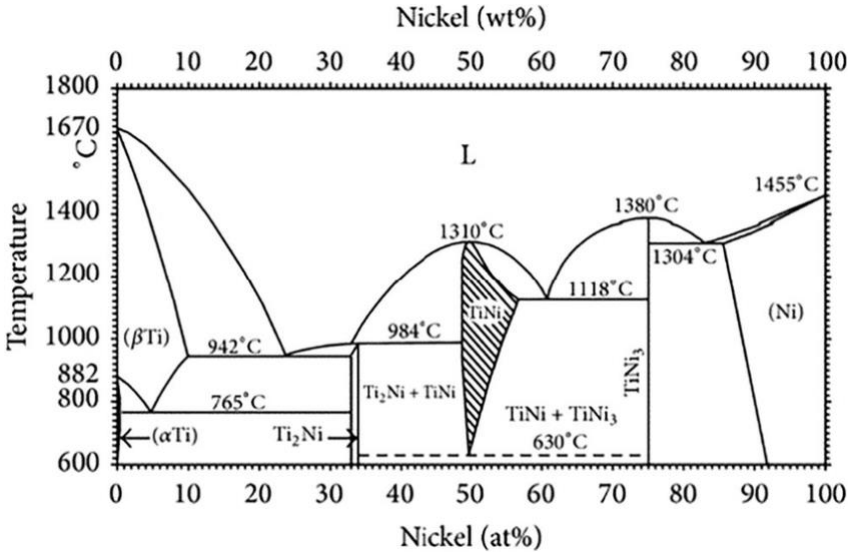

Figure 3: Phase diagram of nickel-titanium binary alloy[11].

v. Superelastic Nitinol

The M_s and M_f temperatures decrease 10°C for every 0.1 at. % Ni was added to the alloy [12]. Shape-memory nitinol alloys tend to have an equal proportion of nickel to titanium, while superelastic nitinol tends to be nickel-rich [7,15]. One common alloy, SE508, uses 50.8 at. % Ni and it has a wrought A_f between -25°C and 5°C [13].

Superelastic nitinol has an austenitic structure at working temperature, and it is used above M_s and A_f. Superelastic nitinol loads and unloads in several, shown in **Figure 4**. When a load is applied to the alloy, there is a period of linear strain. After around 6% strain is induced into the metal, the stress plateaus as the energy goes toward the phase transformation from austenite to martensite [14]. There is some hysteresis, or a delayed change, which causes a permanent set when nitinol is loaded. This hysteresis is attributed to internal friction effects [3], [15].

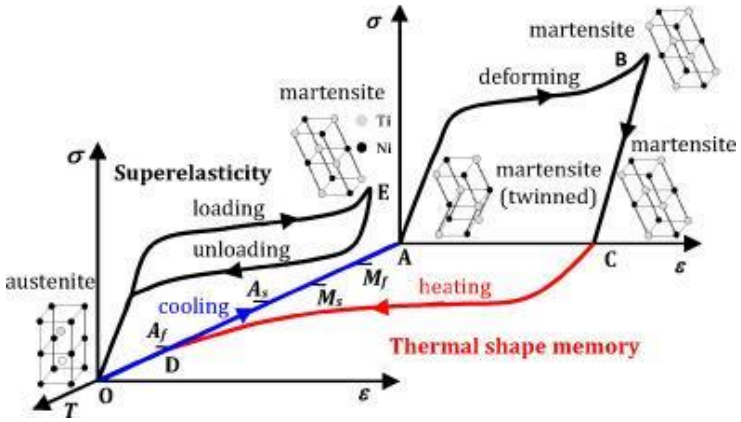

Figure 4: Stress-strain curve of both superelastic and thermal shape memory nitinols with the changes to the microstructure[16].

vi. Shape-Memory Nitinol

For shape-memory alloys, cooling the metal down to working temperature now yields twinned martensite, as previously shown in Figure 4. This occurs when M_s and M_f are above the temperature of application. The transformation is complete at the martensite finish temperature (M_f). Once the alloy is below the M_f temperature, the alloy has shape-memory properties. During loading, there is a similar period of linear strain, followed by a phase-transformation to non-twinned martensite. However, during unloading, the structure does not contain enough energy to return to an austenitic or twinned-martensitic structure. The alloy must be heated above the austenite finish temperature (A_f) to return to its original shape. Increasing the molar ratio of nickel will decrease the martensitic point M_p and austenitic point A_p temperatures [17].

Nitinol Processing

i. Shape Memory Processes

The composition of nitinol is typically an equimolar composition of nickel and titanium. A subtle change to this ratio can have large effects on its properties. Increasing nickel content by even one percent can drastically decrease the material's transformation temperature or increase the austenitic yield strength. This sensitivity can make manufacturing difficult, especially when repeatability and uniformity are necessary. It can also prove to be powerful, as manufacturers can harness precise control in properties and desired transition temperatures [18,19].

Nitinol processing begins by melting raw material ingots by use of vacuum induction melting, then vacuum arc melting. These methods are used due to titanium's high reactivity with oxygen; microstructural homogenization is also achieved. At this stage, the microstructure is not refined enough for the shape memory or elastic properties, and it tends to have a lower fracture resistance. Intermediate materials are made by hot rolling and forging, which are then processed under coldworking and annealing [18,19].

ii. Superelastic Processing

Maximizing superelasticity requires nitinol to be both cold-worked and heat-treated. The first cold-working process requires the nitinol to be drawn to about 50-70% of its original cross-sectional area. Next nitinol is kept under strain during the annealing process—a process called continuous strand strain annealing. This is performed at 450-550^{o}C under a stress of 35-100 MPa, depending on mechanical properties, A_f desired temperature, and cross-sectional area. Due to some shape-memory tendencies in the alloys, the wire would tend to increase in cross-sectional area and decrease in length. For superelastic processing, this tendency is restricted as it reverses the cold-working process. As time goes on and the wire heats up, the strength will drop, and the nitinol will take on a new shape [15].

These processing methods are vital to achieving nitinol's full potential. Nitinol's main applications in the medical industry are reliant on its shape memory and superelastic properties, which will be discussed in the next section.

Applications of Nitinol

Nitinol's predominant use in the engineering world is in the medical device industry, largely because of its biocompatibility, superelasticity, and shape memory properties. Biocompatibility is the ability for a material to be accepted into the body. This property is directly related to the material's corrosion behavior, as well as the tendency to release toxic ions. While nickel is not typically used for internal medical devices, nitinol's formation of a titanium-oxide layer stabilizes its surface layer and forms a physical and chemical boundary to prevent the oxidation of nickel [20].

i. Biocompatibility

Biocompatibility and corrosion resistance are also influenced by mechanical, chemical, electrical, and biological stresses placed on a material. For implanted nitinol devices, understanding the interactions between the surface layer and surroundings is important when considering biocompatibility. Processing can have a dramatic effect on the composition of nitinol's surface layer. Electropolishing is an effective method to remove thermal oxides and nickel accumulated from heat treatments. This generally decreases the possibility of nickel releasing in the short and long term. One common avenue of failure for an in-situ nitinol device is pitting corrosion. Pitting corrosion is an electrochemical reaction, in which oxidation reactions occur at anodic sites and metal ions are released. Localized pits or cavities open in the surface of the device over time. This can result in possible wire fractures, as well as biologically harmful metal ions being released into the surrounding tissue. Pitting has been observed with in situ nitinol devices as early as five months after implantation. This is most likely due to a corrosive surface treatment that rendered the anodic sites vulnerable [20,21]. Another common failure is hydrogen embrittlement, where hydrogen diffuses into the crystal structure and makes the metal harder and more brittle. Much about hydrogen embrittlement in nitinol is unknown, but a

required maximum 50 wt.ppm for wrought ingots is used to comply with ASTM F2063 [2]. After processing, the exact amount hydrogen in a final product is unknown, which will be discussed below.

ii. Stents

Biocompatibility is only one of the properties that is desired in the medical device industry. The mechanical properties prove useful for different applications within this field, including guide wires and heart stents. Nitinol's cyclic mechanical load capabilities are attractive because these devices withstand cyclic loading during their lifetime post-implantation and must be able to return to their original elasticity. Superelastic materials are under constant stress, in which they exhibit constant unloading stress over a large strain. This means the force applied by nitinol is not determined by strain, but by temperature. The flexibility of nitinol is up to ten to twenty times greater than stainless steel (another option for medical devices). High in situ flexibility is a good attribute because of internal pressures that would otherwise cause stents to be crushed. Deformation in stents can lead to serious consequences for their functionality and can put a user's life at risk.

Self-expanding deployment has some advantages compared to conventional stent deployments. Conventional stents and alloys require a balloon to expand the stent. Some drawbacks to this are the stent does not expand as much as nitinol stents, the device requires larger area, and the balloon has an extra chance to rupture and cause the surgery to fail[22]. Using nitinol's shape memory or superelastic properties, a nitinol stent can compress smaller than conventional stents while opening to a larger area with no risk of balloon rupture. The differences are shown in **Figure 5**. In larger arteries like in limbs and heart, this allows for a less intrusive entrance in smaller arteries while expanding to encompass the artery. There are two main types of self-expandable 'shape-memory' stents: thermal and elastic. In a thermal-expanding stent, the device is preloaded in the martensitic phase and positioned in the deployment site, in which the device is warmed by the blood and surrounding tissues and springs back into the desired shape. In contrast, an elastic-expandable stent is compressed to a thin size. Once the stent is positioned, the stent is released and allowed to take the shape of the artery, clearing flow [19-21,23].

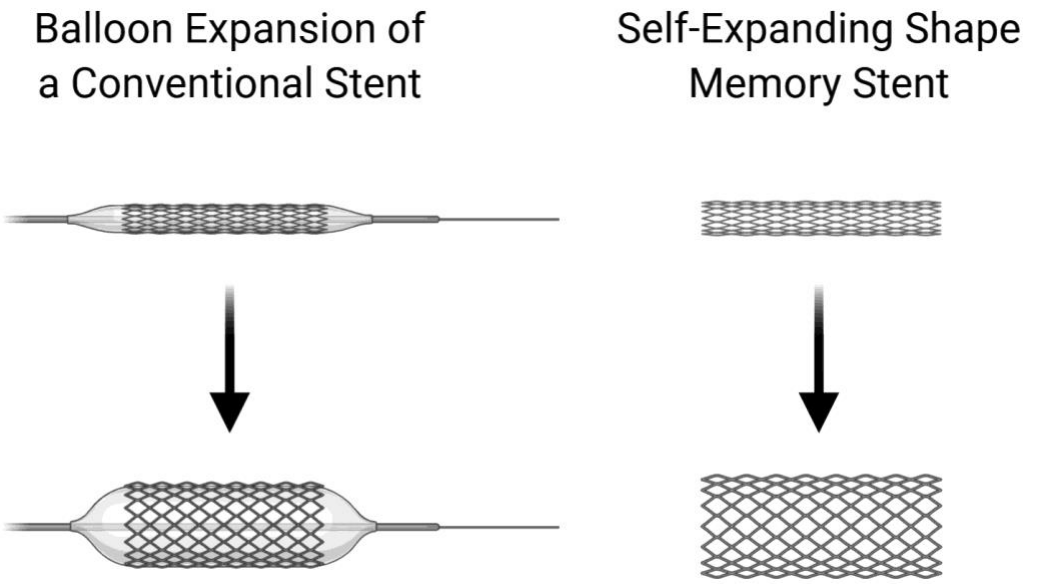

Figure 5: Comparison between balloon expansion for conventional stents and self-expanding stents made from nitinol alloys[23].

Hydrogen Embrittlement

i. Mechanisms of Diffusion

Hydrogen embrittlement is seen throughout many engineering metals, like steels, aluminum, copper, and refractory metals [24-26]. For all metals, hydrogen enters the metal through humidity under a hydrogen atmosphere or an acid and electrochemical processes [26-28]. The latter requires the charging of hydrogen ions:

$$(H^+ + e^- \rightarrow H) \quad (1)$$

For hydrogen to get into the metal, hydrogen needs to first be adsorbed to the metal, which means there is an attraction between the surface and the hydrogen. Only then can the hydrogen be absorbed into the metal. Some hydrogen in the lattice forms into hydrogen gas:

$$(2H \rightarrow H_2) \quad (2)$$

where the gas escapes the metal at the surface. Otherwise, the hydrogen diffuses into the metal lattice, and the concentration builds up. The hydrogen diffusion into the lattice along the plate thickness direction follows Fick's diffusion law:

$$\frac{\partial c}{\partial t} = D\frac{\partial^2 c}{\partial x^2} \quad (3)$$

where *c* is the hydrogen concentration, *t* is the time, *x* is the position, and *D* is the diffusion coefficient [24,28,29].

Oxide layers, like aluminum oxide, can impede the attraction on the surface and decrease the diffusion of hydrogen in the metal. Purposefully oxidizing the metal in a protective salt or oxide is called passivation. Passivation is quite common in the industry, and it has been proven to be biocompatible [30]. Titanium is one of the metals that reacts to form protective oxides and nitrates. A high-level purity is required, and the extra step may not always be convenient in processing [31]. Regardless, hydrogen embrittlement is one of the most complex phenomena to predict due to the unknown kinetics of processes; an applicable predictive physical mechanism model does not yet exist [24].

ii. Hydrogen Testing

The most common form of testing the hydrogen content in nitinol is hot vacuum testing. Adding heat and decreasing pressure can force the hydrogen out of the crystal structure of nitinol; collecting the escaped hydrogen can allow for the precise measurement of hydrogen concentration [32-34]. Because the process is done at high temperatures (>650^{o}C) for extended periods of time, it is a destructive test that limits its use as a quality control step in industry. Due to its light atomic mass, hydrogen cannot be measured with conventional non-intrusive methods, like x-ray fluorescence (XRF).

iii. Hydrogen in Nitinol

According to ASTM F2063-18 and shown in *Table 1*, the maximum wrought concentration of hydrogen is 50 wt.ppm. There is, however, no standard for the concentration of hydrogen after processing due to the destructive nature of hydrogen testing. Observationally, hydrogen embrittlement affects the mechanical properties close to the surface of the metal. Titanium has a much higher affinity for hydrogen than nickel, and it is the primary metal that becomes a hydride. Like oxides and carbides, hydrides in metals are stress concentrators and cause brittle fractures under tension. The concentration of H required to form hydrides is not fully clear, as *Pruitt et al.* cite hydride formation as low as 75 wt.ppm, while *Burch and Mason* tested up to 13000 wt.wpm with no formation of hydride [35]. *Yamanaka et al.* found that hydrogen remains dissolved in a solid solution ($NiTiH_{1.4}$) below 270^{o}C, but above 500^{o}C under a strong hydrogen atmosphere leading to the decomposition of $TiNi_3$ + TiH_2 [36]. Regardless of the formation of hydrides, tensile tests show the areas around the sample, the area that was inflicted by hydrogen, undergo brittle failure at a lower load [37]. In terms of fatigue, low loading (1.4% strain) and low cycling ($<10^4$) were not greatly impacted by hydrogen up to 80 wt.ppm [38]. To test for the effects of hydrogen on nitinol, many groups offered different methods of hydrogenation. *Yokoyama et al.* used an acidulated phosphate solution (APF), which was made of H_3PO_4 and a fluoride salt. They managed to get a range of hydrogen concentrations from 100-1000 wt.ppm [39] *Pruitt et al.* used 85% H_3PO_4 at various times at 80^{o}C and found hydrides above 583 wt.ppm, while *Pelton et al*. used an unlisted concentration of H_3PO_4 for a maximum of 20 minutes at 90^{o}C [36,38]. The effects of tensile properties are missing from studies, however.

Experimental Design

In this study, the goal is to understand and determine the effects of the concentration of hydrogen in SE508 nitinol wire regarding strength, permanent set, ductility, and mode-of-failure of the fracture surface. Tensile testing will show how the strength and permanent set degrades with higher hydrogen concentrations. Observing the fracture surfaces of samples at different levels of hydrogen is important for showing how hydrogen has affected the local plastic deformation.

A preliminary test was conducted to determine how fast 50% sulfuric acid adds hydrogen into the microstructure at room temperature. Because the trend was unknown during the preliminary test, periods of 1 minute, 2 minutes, 5 minutes, 10 minutes, 20 minutes, 1 hour, 1 day, and 3 days in the sulfuric acid were chosen. Using hot vacuum extraction, the exact hydrogen content was found at each interval, shown in **Figure 6**.

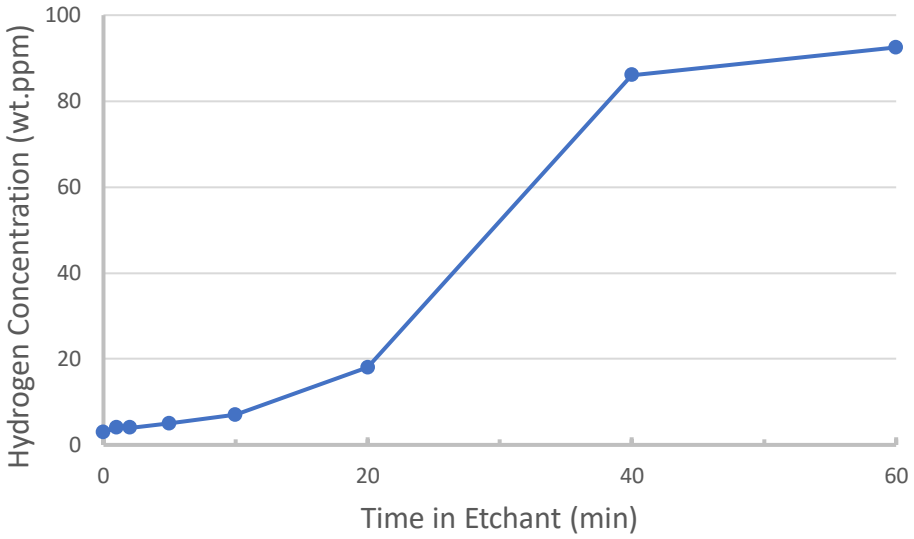

Figure 6: Preliminary etch of superelastic nitinol in 50% sulfuric acid.

It was determined the time of interest was primarily between 10 and 60 minutes. 10-minute intervals within that time will give further understanding of multiple hydrogen concentrations. For the strongest statistical significance possible with limited testing time, there were five samples submerged in the sulfuric acid at each of these time levels, as well as a control group. The hydrogen concentrations of these samples are displayed below in **Figure 7**.

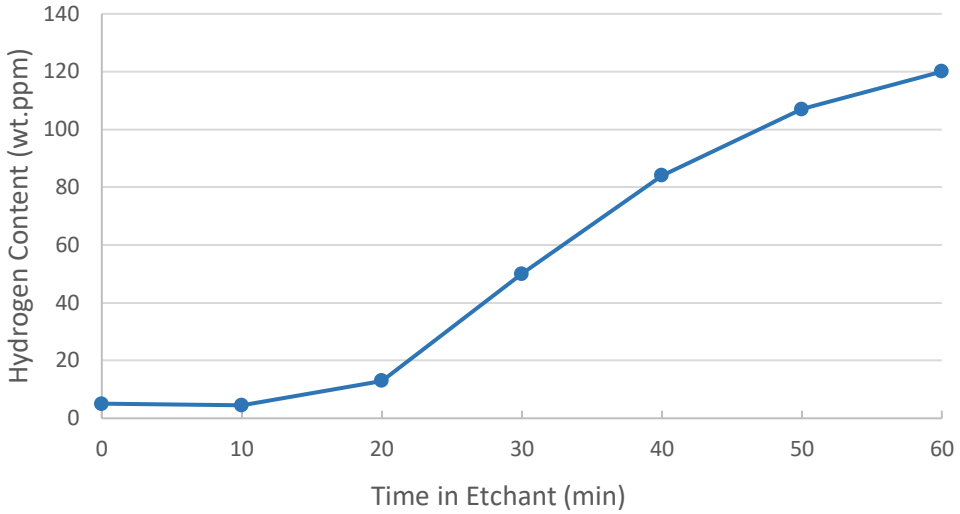

Figure 7: Final etch of superelastic nitinol in 50% sulfuric acid.

Three samples were submerged in the sulfuric acid for one day, and three more samples were submerged for four days to observe the effects of higher hydrogen concentrations. The samples had hydrogen concentrations of 125 wt.ppm and 143 wt.ppm, respectively.

The next step in this experiment was to tensile test each sample on a 50kN Instron as per ASTM F2516 standard for tension testing superelastic nitinol. This standard requires 150 mm of wire between each clamp, so the samples were cut down to size using large wire cutters. The cross-head displacement rate was set to 5 mm/min. The samples were loaded and pulled to 6% strain, then returned to zero strain as per the ASTM standard. This process allows for a measurement of permanent set, which was found by taking the difference in strain from when the initial and final load read above 7MPa. The samples were then tested to fracture, where the maximum elongation and ultimate tensile stress were recorded.

To further investigate the effects of hydrogen concentration on the nitinol wire samples, the fracture surface of one sample from each hydrogen level was imaged under the SEM. The spot size was set to 4.5 and the accelerating voltage was set to 20.0 kV consistently. The cross-section of the fracture surface was observed at a low magnification around 90x as well as a higher magnification around 3000x to observe any reduction of area and surface artifacts present.

Results

i. Tensile Tests

The acid had noticeable, visible effects to the nitinol wire. Shown in **Figure 8**, the evolution of the appearance of the wires are shown. At first, the black oxide layer is clearly seen. Between 40 and 60 minutes, the oxide completely disappears, with possible evidence of pitting shown. Some more pitting can somewhat be seen in the 48-hour sample, but it does appear that pitting becomes a larger problem. This has the potential to affect the tensile properties, as pits act

as a stress concentrator and may cause fractures sooner. If there are noticeable effects between the levels, further analysis would be needed to identify if pitting impacted the tensile properties or if it was hydrogen changing the microstructure.

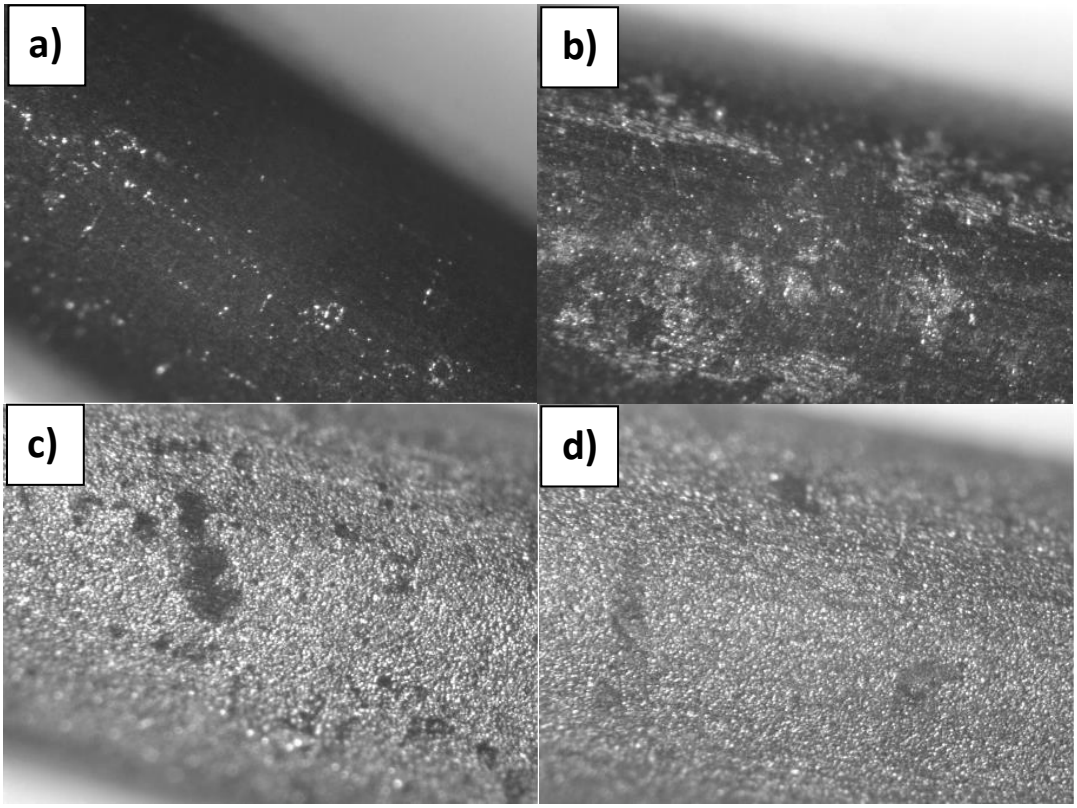

Figure 8: The impact of the acid on the nitinol surface at a) 20 minutes, b) 40 minutes, c) 60 minutes, d) 24 hours.

The results found from our tensile tests show us the correlation between the hydrogen content of the nitinol samples and their tensile properties. The time periods between 0 and 60 minutes had a sample size of five, while the one-day and four-day samples each had three test wires. The permanent set data is displayed in **Figure 9**. Again, there were five samples at each hydrogen concentration level through 120, and three samples at 125 and 145 wt.ppm. The red data points represent an average value of these samples. It can be observed that there is some variance at each level, but there does not seem to be a correlation with hydrogen concentration and that variance. In comparison to different concentrations, the mean of each data set above and below the 50 wt.ppm ASTM limit for wrought nitinol shows little difference in value.

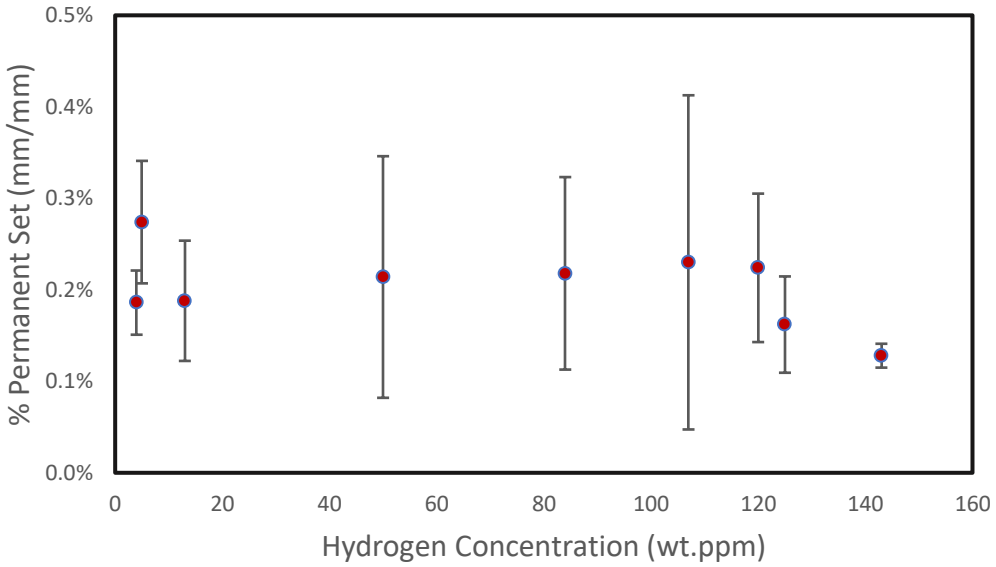

Figure 9: Impact of hydrogen concentration on permanent set. One standard deviation is shown in the error bounds.

The ultimate tensile strength, shown in **Figure 10**, remained around 1180 MPa, which matched the specifications of the manufacturer. The samples with low hydrogen concentration had low variance, with all five samples fracturing with 5 MPa of each other. Any hydrogen added to the system seemed to increase the spread of tensile strengths. Although more variance in tensile strength may be of concern, the spread only minimally increased with the one-day sample having a standard deviation of 20 MPa.

In addition, the tensile strength generally increased as more hydrogen entered the crystal structure. The trend is subtle, and the increase of tensile strength would be unnoticeable when applying the nitinol wire. Importantly, the tensile strength did not decrease as hydrogen entered the wire.

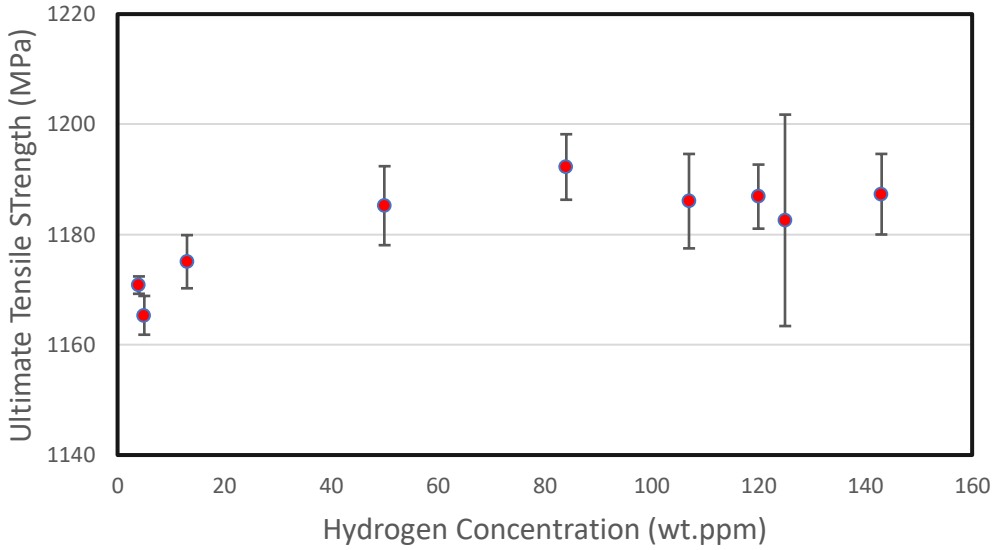

Figure 10: Ultimate tensile strength of nitinol samples at each hydrogen content.

The final variable measured is maximum elongation. A large impact on ductility could signal that hydrogen embrittlement is happening at these concentrations. However, a large change in ductility was not observed, shown in **Figure 11**. The overall ductility hovered around 19.0% strain from control to 143 wt.ppm. Likely due to the limited number of samples, no decisive conclusion can be made about the correlation between maximum strain and hydrogen concentration. Regardless, any loss in strain, even in the high concentrations, would not be indicative of an embrittled part.

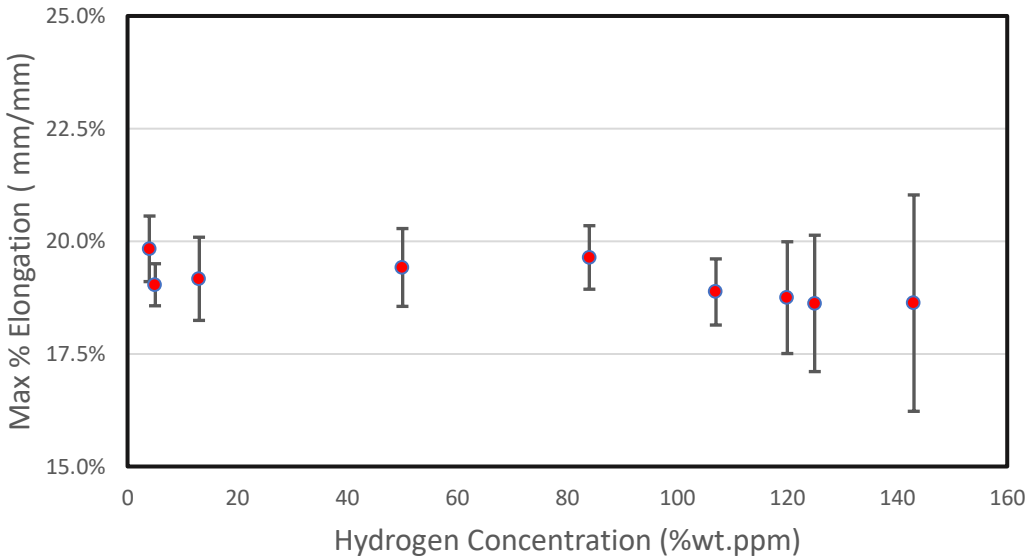

Figure 11: Maximum percent elongation of nitinol samples at each hydrogen concentration.

ii. SEM Imaging

The SEM images taken in this experiment helped determine the variable most affected by hydrogen content. Upon visual inspection of each sample, there was obvious necking for the samples containing up to 120 wt.ppm hydrogen, indicating a ductile failure. The samples that had been left in the etchant for one and four days (125 and 142.5 wt.ppm) did not show signs of necking. Looking at the cross-section of the control sample compared to the cross-section of the most hydrogenated sample in **Figure 12**, there is a change in reduction of area.

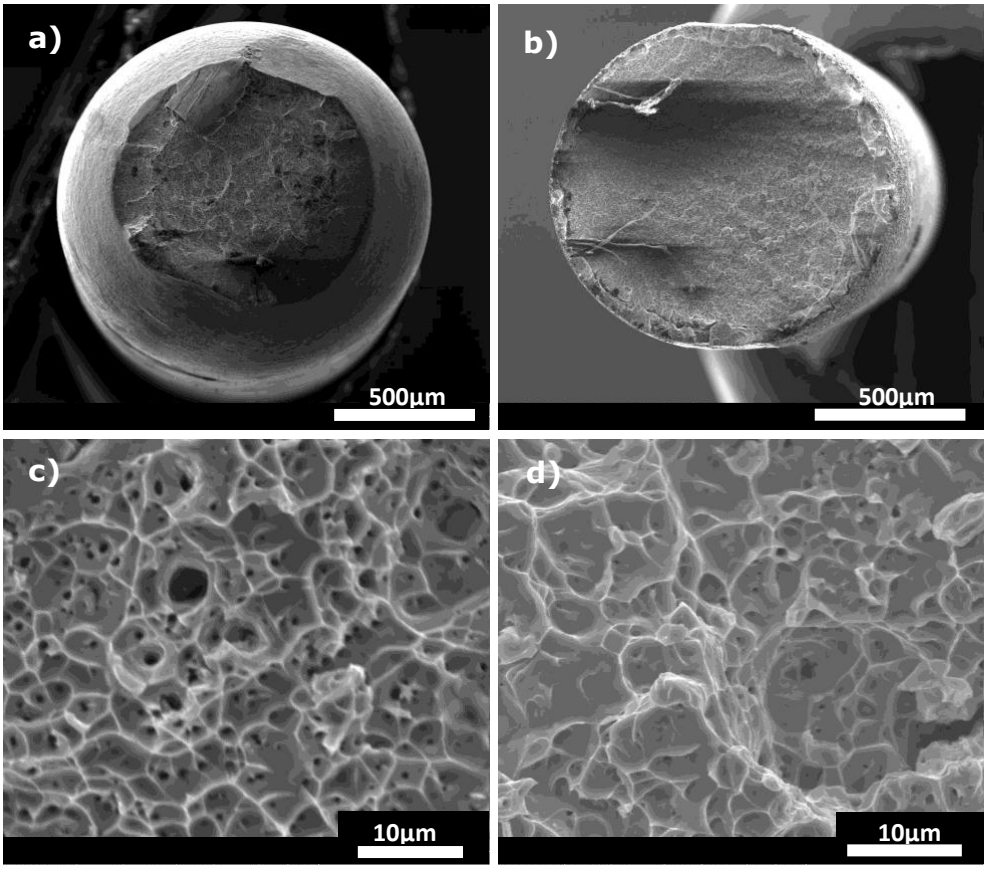

Figure 12: SEM images of nitinol wire fracture surfaces after tensile testing. (a) Fracture surface of control sample (5 wt.ppm hydrogen) with obvious necking, (b) fracture surface of most hydrogenated sample (142.5 wt.ppm hydrogen) with no reduction of area, (c) higher magnification of control sample with microvoid coalescence, (d) higher magnification of 142.5 wt.ppm sample with microvoid coalescence.

In the higher magnification images displayed in **Figure 12**, there is evidence of micro-void coalescence in both the control sample and 142.5 wt.ppm sample. This is an indicator of a ductile failure. In the highly hydrogenated sample, however, there are other surface artifacts visible that suggest this mode of failure was mixed, and that it failed with more brittleness than the control sample. The SEM images of the additional samples can be viewed in **Appendix A**. All SEM images of samples that were in the etchant up to one hour are visually similar to the control sample, and the other sample beyond that threshold is visually similar to the 142.5 wt.ppm sample.

Discussion

i. Tensile Tests

The data collected from the tensile tests indicate that there was no major negative effect of hydrogen concentration on the superelastic nitinol wires. In permanent set, the hydrogen concentration did not change the deformation of the wire after loading to 6% strain. Statistical T-tests were performed to support this, as shown in **Figure 13**. Each hydrogen level is compared to the control sample. Most of the p-values lie above 0.05, so the null hypothesis cannot be rejected. Therefore, hydrogen content had no statistical effect on the permanent set of the nitinol wire samples.

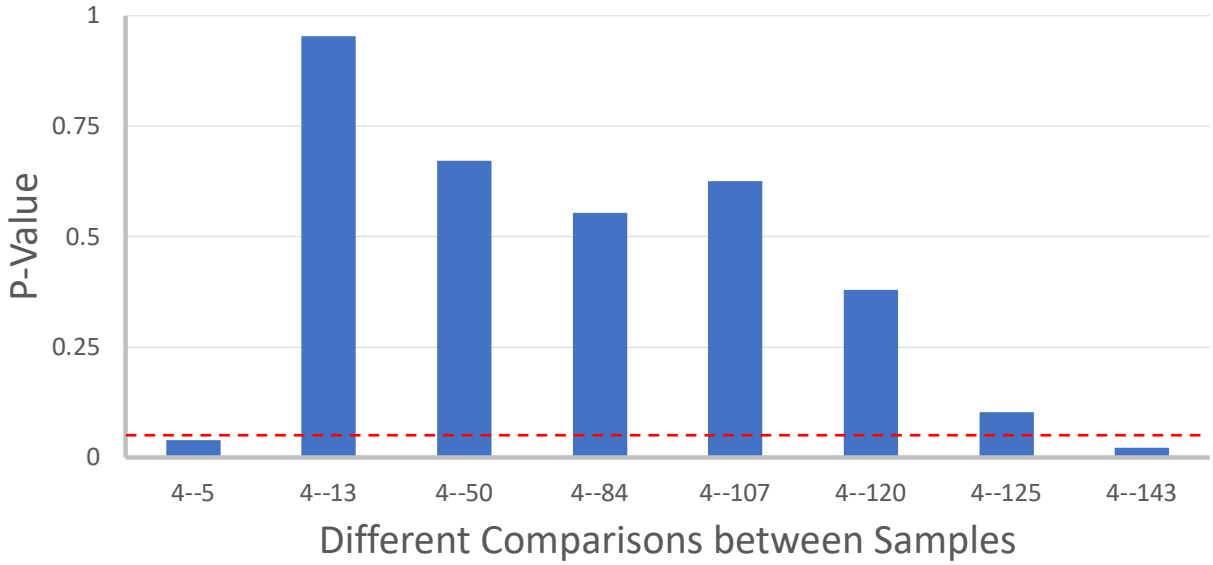

Figure 13: Statistical T-tests comparing samples at each hydrogen level to the control sample (4 wt.ppm) for permanent set data. The second number represents the concentration of hydrogen that was compared to the sample. The red line signals the inability to reject the null hypothesis if above.

Likewise, the ultimate tensile strength of the nitinol wires showed little variance between hydrogen content levels. Another T-test was performed to support this, shown in **Figure 14**. For ultimate tensile strength, most of the p-values lie below 0.05, and the null hypothesis can be rejected, meaning there is a statistical effect of hydrogen content on the UTS. Based on the trend in **Figure 10**, however, it can be observed that this is not a negative effect. In fact, the UTS increases (though minimally) above the 50 wt.ppm ASTM limit for wrought nitinol up to 143 wt.ppm.

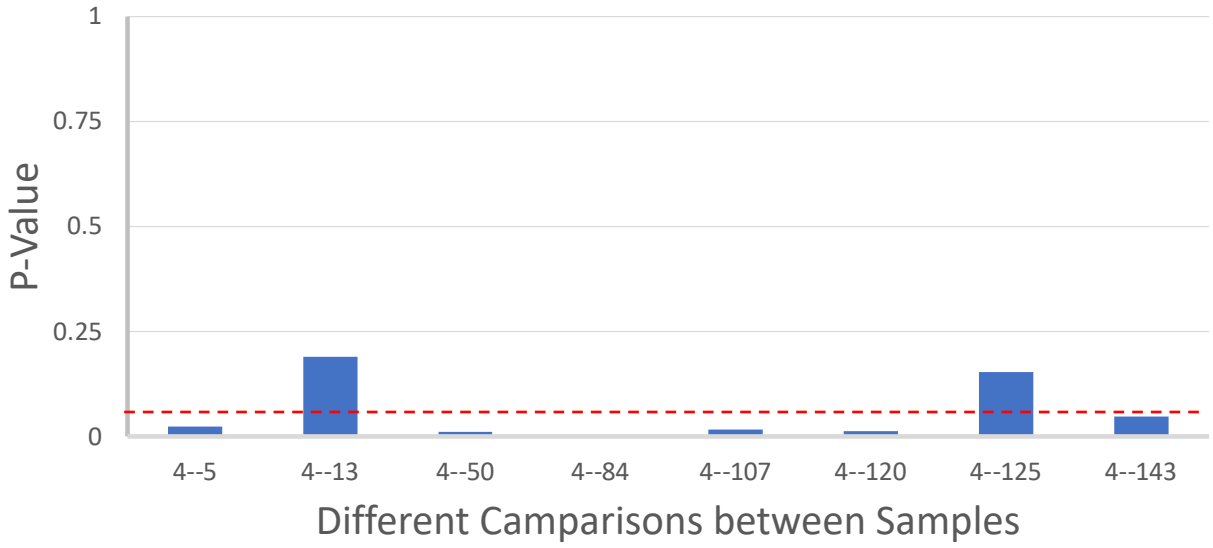

Figure 14: Statistical T-tests comparing samples at each hydrogen level to the control sample for ultimate tensile strength data. Because most samples are below the red line, the null hypothesis can be rejected.

ii. SEM Imaging

Upon inspection of the SEM images collected, local plastic deformation was the most impacted by increasing hydrogen content. This is indicated by the significant decrease in reduction of area beyond a hydrogen concentration of 120 wt.ppm. This means that at higher hydrogen levels, these wires will not deform before they break, and will break much faster when failure begins. This can lead to a more catastrophic failure of a component made from this superelastic nitinol. The reduction of area trend is displayed below in **Figure 15**.

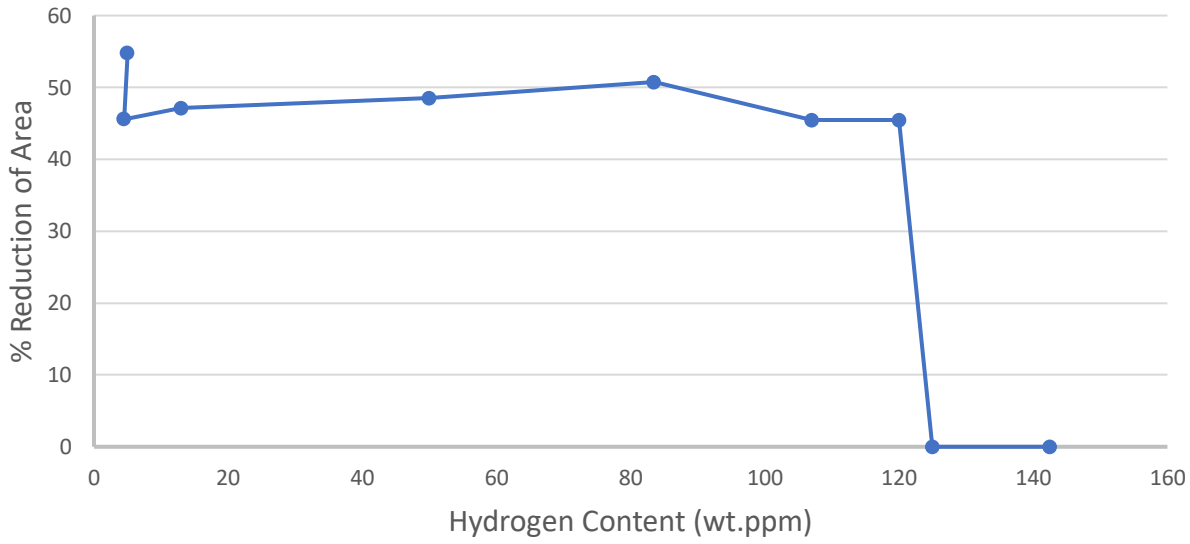

Figure 15: The reduction of area determined from SEM imaging at each level.

The presence of micro-void coalescence in samples at all hydrogen levels is indicative of ductile fracture. Without necking, however, this does little to make up for a loss in plastic deformation. Additionally, the presence of other surface artifacts shows there was potentially a mixed mode of failure for the highly hydrogenated samples.

Conclusions

1. According to tensile testing data, permanent set of the nitinol wire was not impacted by the addition of hydrogen. Throughout the testing, all the samples had around .20% permanent set, with no sample not passing the .5% ASTM F2516 threshold.
2. Ultimate tensile strength saw a subtle increase as more hydrogen diffused through the wires. Note this is only below 150 wt.ppm, and no conclusions can be made outside of this region.
3. Maximum elongation saw a slight decrease in the mean but is within the margin of error. The decrease does not play a significant role in industrial processes.
4. There was an evolution of the mode-of-failure of the fracture surface under the SEM. All low-hydrogen samples had only micro-void coalescence with samples above 140 wt.ppm experiencing some different artifacts.
5. There was a reduction in the area that disappeared between 120 wt.ppm and 125 wt.ppm. Further research will be needed to show whether that reduction is from hydrogen, pitting, or time in etchant.

Recommendations

1. To be sure that processed nitinol can truly withstand more than 50 wt.ppm hydrogen, other mechanical, thermal, and chemical properties should be analyzed. This will allow for a wider scope of understanding of how hydrogen affects superelastic nitinol beyond the ASTM limit.
2. Long-term fatigue testing should be conducted as hydrogen can decrease the lifetime in other alloys. This is important because medical devices like stents are intended to not break over an extended amount of time.
3. The fracture behavior and artifacts found on the surface could indicate a more brittle fracture. A further exploration is needed to understand if these differences are of concern, as the local plastic deformation was most impacted by hydrogen content in this study.

References

[1] G. B. KAUFFMAN and I. MAYO, “The Story of Nitinol: The Serendipitous Discovery of the Memory Metal and Its Applications,” The Chemical Educator, vol. 2, no. 2, pp. 1–21, Jun. 1997, doi: 10.1007/s00897970111a

[2] “Standard Specification for Wrought Nickel-Titanium Shape Memory Alloys for Medical Devices and Surgical Implants 1”, doi: 10.1520/F2063-18.

[3] D. Hodgson and S. Russell, “Nitinol melting, manufacture and fabrication,” Minimally Invasive Therapy & Allied Technologies, vol. 9, no. 2, pp. 61–65, Jan. 2000, doi: 10.3109/13645700009063051.

[4] B. JosØ María Gallardo Fuentes, P. Gümpel, J. Strittmatter, P. Gümpel, J. Strittmatter, and J. M. Gallardo Fuentes, “Phase Change Behavior of Nitinol Shape Memory Alloys Influence of Heat and Thermomechanical Treatments.”

[5] A. Toro, F. Zhou, M. H. Wu, W. Van Geertruyden, and W. Z. Misiolek, “Characterization of Non-Metallic Inclusions in Superelastic NiTi Tubes,” J Mater Eng Perform, vol. 18, no. 5–6, pp. 448–458, Aug. 2009, doi: 10.1007/s11665-009-9410-1.

[6] J. Eaton-Evans, J. M. Dulieu-Barton, E. G. Little, and I. A. Brown, “Observations during mechanical testing of Nitinol,” Proc Inst Mech Eng C J Mech Eng Sci, vol. 222, no. 2, pp. 97–105, Feb. 2008, doi: 10.1243/09544062JMES797.

[7] “Standard Test Method for Transformation Temperature of Nickel-Titanium Alloys by Thermal Analysis 1”, doi: 10.1520/F2004-17.

[8] T. G. Bradley, W. A. Brantley, and B. M. Culbertson, “Differential Scanning Calorimetry (DSC) Analyses Of Superelastic And Nonsuperelastic Nickel-Titanium Orthodontic Wires,” 1996.

[9] C. D. Cirstea, F. Tolea, D. Patroi, V. Cirstea, and V. Tsakiris, “SOME ASPECTS REGARDING PRECIPITATES IN THE NiTi SHAPE MEMORY MATERIALS,” 2022.

[10] E. Marchenko, G. Baigonakova, K. Dubovikov, O. Kokorev, Y. Yasenchuk, and A. Vorozhtsov, “In Vitro Bio-Testing Comparative Analysis of NiTi Porous Alloys Modified by Heat Treatment,” Metals (Basel), vol. 12, no. 6, Jun. 2022, doi: 10.3390/met12061006.

[11] S. Hellberg, J. Hummel, P. Krooß, T. Niendorf, and S. Böhm, “Microstructural and mechanical properties of dissimilar nitinol and stainless steel wire joints produced by micro electron beam welding without filler material,” Welding in the World, vol. 64, no. 12, pp. 2159–2168, Dec. 2020, doi: 10.1007/s40194-020-00991-3.

[12] J. C. Chekotu, R. Groarke, K. O'Toole, and D. Brabazon, "Advances in selective laser melting of Nitinol shape memory alloy part production," Materials, vol. 12, no. 5. MDPI AG, 2019. doi: 10.3390/MA12050809.

[13] "Material Data Sheet Superelastic Nitinol".

[14] N. E. Waters, "Superelastic Nickel-titanium Wires," Br J Orthod, vol. 19, no. 4, pp. 319–322, Nov. 1992, doi: 10.1179/bjo.19.4.319.

[15] A.R. Pelton, J. DiCello, and S. Miyazaki, "Optimisation of processing and properties of medical grade Nitinol wire," Min Invas Ther & Allied Technologies, vol. 9(1), pp. 107–118, 2000.

[16] J. W. Mwangi, H. Zeidler, R. Kühn, A. Schubert, and J. W. Mwangi, "Suitability assessment of micro-EDM in machining Nitinol for medical applications," 2016. [Online]. Available: www.euspen.eu

[17] K. Kuś, T. Breczko, and K. Kus, "DSC-investigations of the effect of annealing temperature on the phase transformation behaviour in Ni-Ti shape memory alloy," 2010. [Online]. Available: https://www.researchgate.net/publication/267947401

[18] D. Kapoor, "Nitinol for Medical Applications: A Brief Introduction to the Properties and Processing of Nickel Titanium Shape Memory Alloys and their Use in Stents," Johnson Matthey Technology Review, vol. 61, no. 1, pp. 66–76, Jan. 2017, doi: 10.1595/205651317X694524.

[19] A. Concilio and L. Lecce, Shape Memory Alloy Engineering. Oxford, UK, 2015.

[20] S. Nagaraja, R. Brown, D. Saylor, and A. Undisz, "Oxide Layer Formation, Corrosion, and Biocompatibility of Nitinol Cardiovascular Devices," Shape Memory and Superelasticity, vol. 8, no. 2, pp. 45–63, Jun. 2022, doi: 10.1007/s40830-022-00365-2.

[21] T. Duerig, A. Pelton, and D. Stöckel, "An overview of nitinol medical applications," Materials Science and Engineering: A, vol. 273–275, pp. 149–160, Dec. 1999, doi: 10.1016/S0921-5093(99)00294-4.

[22] S.-Y. Lee, "The Significance of Self-Expandable Stents in Patients with Congenital Heart Disease in Current Era," Korean Circ J, vol. 49, no. 10, p. 943, 2019, doi: 10.4070/kcj.2019.0201.

[23] H. Holman, M. N. Kavarana, and T. K. Rajab, "Smart materials in cardiovascular implants: Shape memory alloys and shape memory polymers," Artif Organs, vol. 45, no. 5, pp. 454–463, May 2021, doi: 10.1111/aor.13851.

[24] A. V. Bochkaryova, Y. V. Li, S. A. Barannikova, and L. B. Zuev, "The effect of hydrogen embrittlement on the mechanical properties of aluminum alloy," in IOP Conference

Series: Materials Science and Engineering, Institute of Physics Publishing, 2015. doi: 10.1088/1757-899X/71/1/012057.

[25] M. B. Djukic, V. S. Zeravcic, G. Bakic, A. Sedmak, and B. Rajicic, “Hydrogen Embrittlement of Low Carbon Structural Steel,” Procedia Materials Science, vol. 3, pp. 1167–1172, 2014, doi: 10.1016/j.mspro.2014.06.190.

[26] Z. Feng, X. Li, X. Song, T. Gu, and Y. Zhang, “Hydrogen Embrittlement of CoCrFeMnNi High-Entropy Alloy Compared with 304 and IN718 Alloys,” Metals (Basel), vol. 12, no. 6, p. 998, Jun. 2022, doi: 10.3390/met12060998.

[27] A. Matting and R. Ziegler, “Brittleness in Copper and Copper Alloys With Particular Reference to Hydrogen Embrittlement,” in ASM Failure Analysis Case Histories: Processing Errors and Defects, ASM International, 2019. doi: 10.31399/asm.fach.process.c9001447.

[28] R. P. Frohmberg, W. J. Barnett, and A. R. Troiano, “"i;;i* •:C DELAYED FAILURE AND HYDROGEN EMBRITTLEMENT IN STEEL.”

[29] J. R. Scully, G. A. Young, and S. W. Smith, “Hydrogen embrittlement of aluminum and aluminum-based alloys,” in Gaseous Hydrogen Embrittlement of Materials in Energy Technologies, Elsevier, 2012, pp. 707–768. doi: 10.1533/9780857093899.3.707.

[30] Paul Kovacs and James Davidson, “Passivation method and passivation implant,” European Patent Office, Jun. 1992.

[31] B. W. Callen, B. F. Lowenberg, S. Lugowski, R. N. S. Sodhi, and J. E. Davies, “Nitric acid passivation of Ti6A14V reduces thickness of surface oxide layer and increases trace element release,” J Biomed Mater Res, vol. 29, no. 3, pp. 279–290, Mar. 1995, doi: 10.1002/jbm.820290302.

[32] V. C. F. Holm and J. G. Thompson, “DETERMINATIONS OF HYDROGEN IN FERROUS MATE~ RIALS BY VACUUM EXTRACTION AT 800° C AND BY VACUUM FUSION,” 1941.

[33] R. A. Yeaton, “The vacuum fusion technique as applied to the analysis of gases in metals,” Vacuum, vol. 2, no. 2, pp. 115–124, Apr. 1952, doi: 10.1016/0042-207X(52)90456-9.

[34] G. A. Bickel, L. W. Green, M. W. D. James, T. G. Lamarche, P. K. Leeson, and H. Michel, “The determination of hydrogen and deuterium in Zr–2.5Nb material by hot vacuum extraction mass spectrometry,” Journal of Nuclear Materials, vol. 306, no. 1, pp. 21–29, Nov. 2002, doi: 10.1016/S0022-3115(02)01230-8.

[35] R. Burch and N. B. Mason, “Absorption of hydrogen by titanium–cobalt and titanium–nickel intermetallic alloys. Part 1.—Experimental results,” Journal of the Chemical

Society, Faraday Transactions 1: Physical Chemistry in Condensed Phases, vol. 75, no. 0, p. 561, 1979, doi: 10.1039/f19797500561.

[36] A. Pelton et al., “Structural and Diffusional Effects of Hydrogen in TiNi,” 2003. [Online]. Available: www.nitinol.com

[37] V. P. Iasnii, O. Z. Student, and H. M. Nykyforchyn, “Influence of Hydrogenation on the Character of Fracture of Nitinol Alloy in Tension,” Materials Science, vol. 55, no. 3, pp. 386–391, Nov. 2019, doi: 10.1007/s11003-019-00314-y.

[38] J. Sheriff, A. R. Pelton, and L. A. Pruitt, “Hydrogen Effects on Nitinol Fatigue,” 2004. [Online]. Available: www.nitinol.com

[39] K. Yokoyama, K. Kaneko, K. Moriyama, K. Asaoka, J. Sakai, and M. Nagumo, “Hydrogen embrittlement of Ni-Ti superelastic alloy in fluoride solution,” J Biomed Mater Res, vol. 65A, no. 2, pp. 182–187, May 2003, doi: 10.1002/jbm.a.10457.

Appendix A

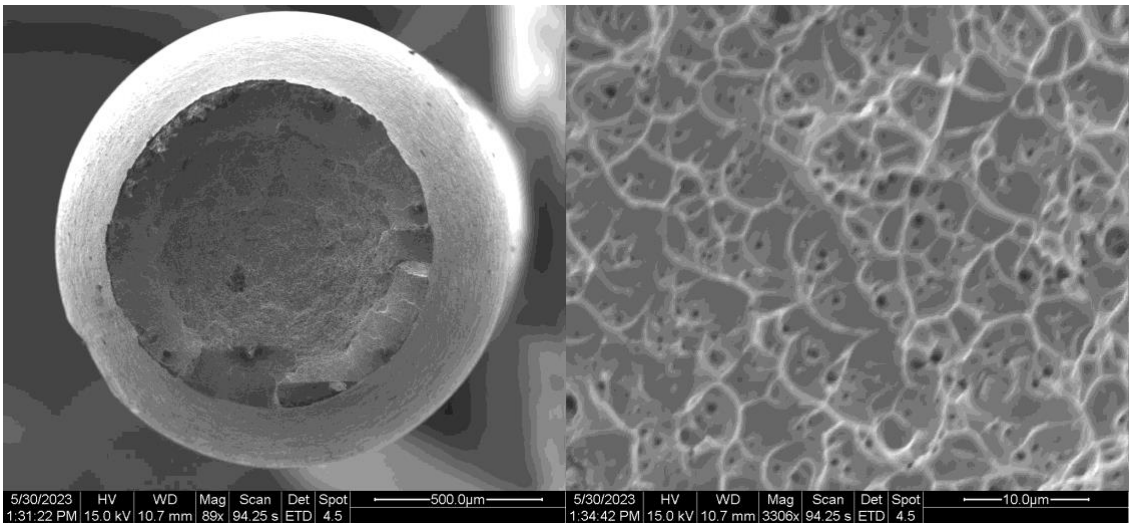

Figure A1: Low magnification (left) and high magnification (right) SEM image of fracture surface of superelastic nitinol wire etched in 50% sulfuric for 20 minutes and tensile tested.

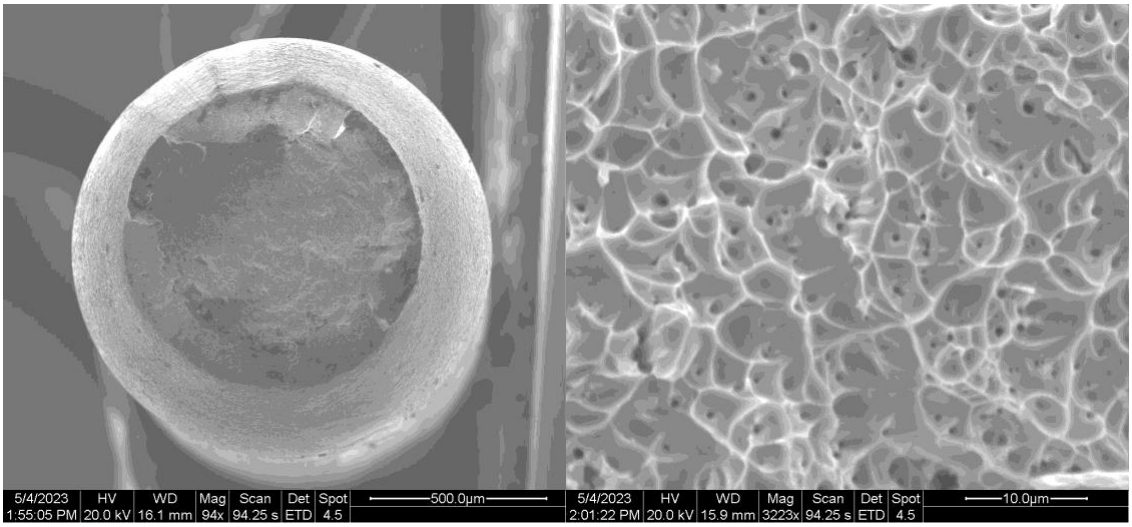

Figure A2: Low magnification (left) and high magnification (right) SEM image of fracture surface of superelastic nitinol wire etched in 50% sulfuric for 30 minutes and tensile tested.

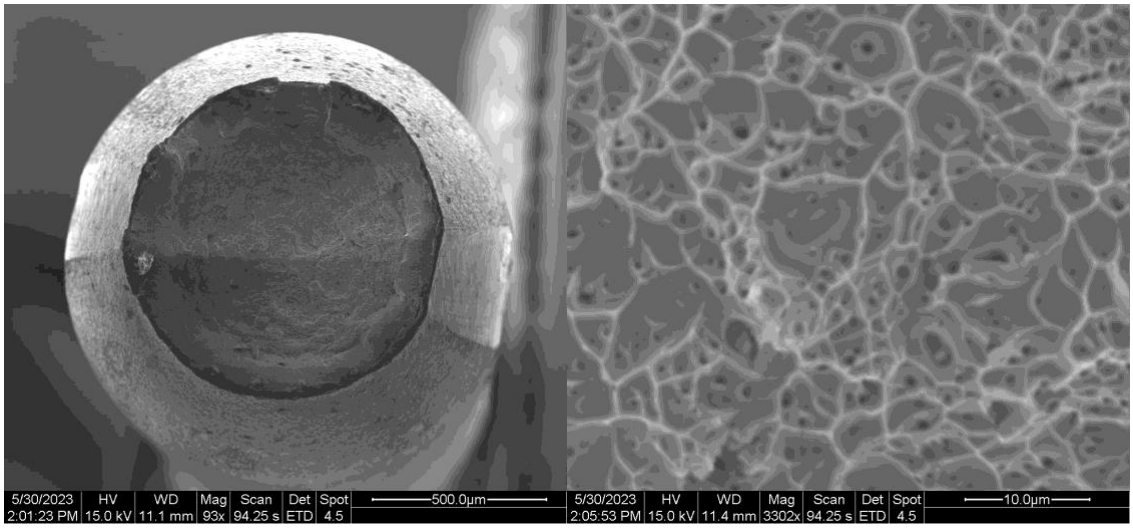

Figure A3: Low magnification (left) and high magnification (right) SEM image of fracture surface of superelastic nitinol wire etched in 50% sulfuric for 40 minutes and tensile tested.

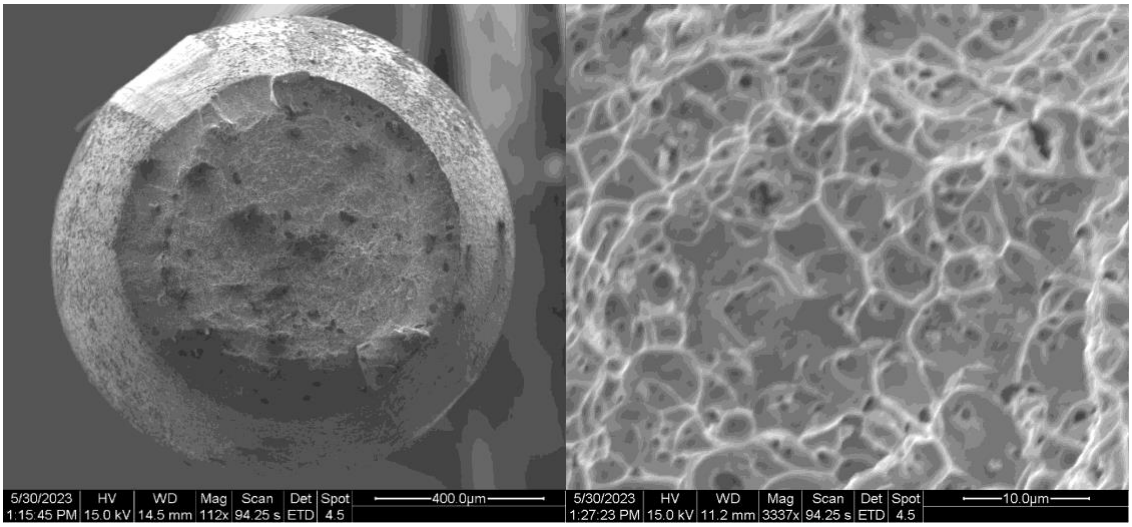

Figure A4: Low magnification (left) and high magnification (right) SEM image of fracture surface of superelastic nitinol wire etched in 50% sulfuric for 50 minutes and tensile tested.

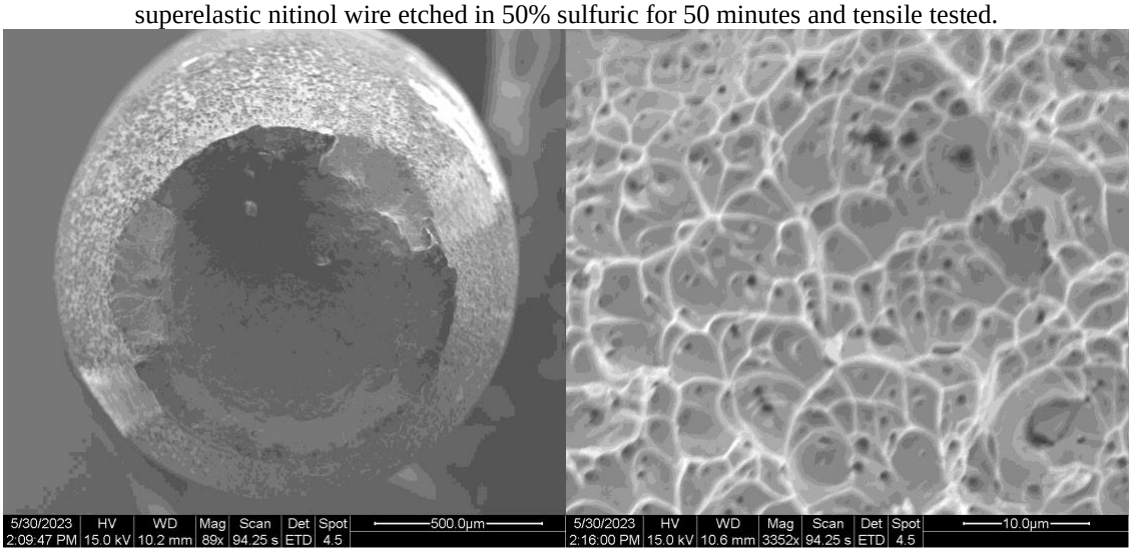

Figure A5: Low magnification (left) and high magnification (right) SEM image of fracture surface of superelastic nitinol wire etched in 50% sulfuric for 60 minutes and tensile tested.

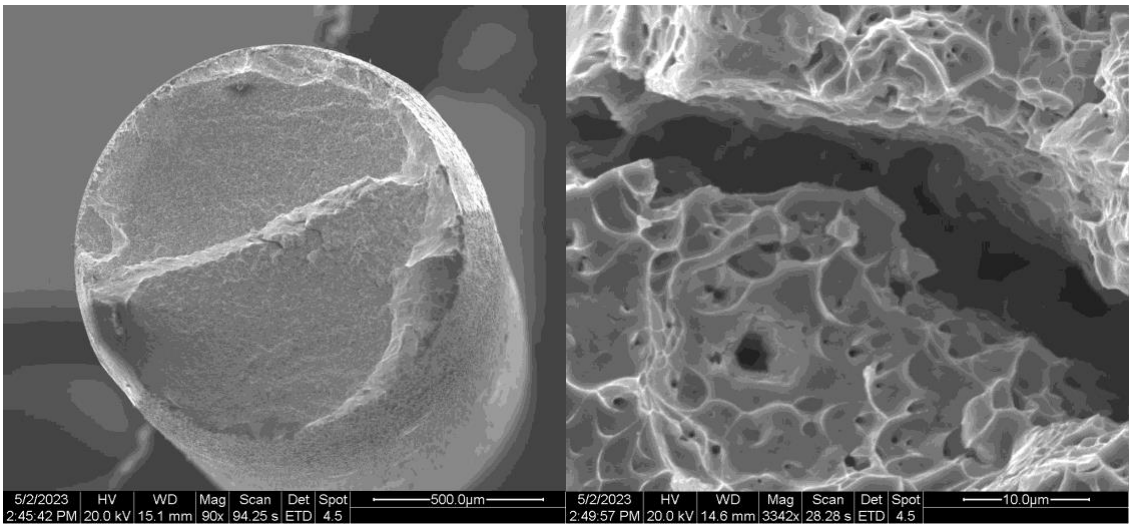

Figure A6: Low magnification (left) and high magnification (right) SEM image of fracture surface of superelastic nitinol wire etched in 50% sulfuric for one day and tensile tested.